ChemComm

COMMUNICATION

View Article Online
View Journal | View Issue

Cite this: *Chem. Commun.*, 2019, 55, 790

Received 28th September 2018,
Accepted 7th December 2018

DOI: 10.1039/c8cc07768a

rsc.li/chemcomm

Pyrrolopyrrole aza-BODIPY near-infrared photosensitizer for dual-mode imaging-guided photothermal cancer therapy†

Chaolong Wu,[a] Xiaoyu Huang,[a] Yunyun Tang,[a] Wanyue Xiao,[a] Liguo Sun,*[b] Jinjun Shao *[a] and Xiaochen Dong *[a]

A NIR photosensitizer pyrrolopyrrole aza-BODIPY (PPAB) was synthesized in a straightforward manner. Through the use of PPAB NPs as a photothermal agent, photoacoustic imaging (PAI) and NIR fluorescence imaging (NIR-FI) can be achieved *in vivo*. In addition, the photothermal ablation of tumor cells can be realized both *in vitro* and *in vivo*, even at a low concentration (0.5 mg kg^{-1}).

Cancer remains one of the biggest threats to human health among human diseases although massive efforts have been implemented to conquer its various forms.[1–4] So far, photothermal therapy (PTT) has been developed as an efficient cancer therapeutic method to overcome the drawbacks of conventional treatments due to its low toxicity, low side effects, minimal invasiveness, and particularly no drug resistance.[5–7] PTT mainly uses photosensitive agents capable of absorbing electromagnetic radiation (close to infrared wavelengths). After interacting with electromagnetic radiation, the electrons of photothermal agents jump from the ground state (S_0) to the excited state (S_1). Energy relaxation then occurs through non-radiative attenuation, resulting in a heat release that is used to kill the tumor cells.[8] As a result, photothermal agents with high photothermal conversion (PTC) efficiency could reduce the suffering and remedy cycles during PTT.[9] Nevertheless, it is necessary to employ an appropriate imaging technique to guide the distribution of phototherapy agents *in vivo* during PTT.[5,10–12] Photoacoustic imaging (PAI), a newly developed imaging modality, not only provides an optional imaging modality for tumor diagnosis, but also can be used to assist with surgery operation. Recently, PAI has attracted great attention owing to its advantages of high optical contrast, deep tissue penetration, and high spatial resolution.[13] Additionally, near-infrared fluorescence imaging (NIR-FI) is often applied in PTT for real-time monitoring the accumulation and metabolism of photothermal agents *in vivo* at tumor sites.[6] Hence, it is urgent to explore an excellent photosensitizer with intense NIR absorption as well as simultaneous PAI and NIR-FI performance for cancer therapy.

In the past few decades, various inorganic materials such as gold-based nanostructures,[14–16] transition metal sulfide nanostructures,[17–19] and carbon-based nanomaterials (such as carbon nanotubes and graphene)[20] have been developed as photothermal agents for PTT. However, the clinical applications of these inorganic materials are limited by their low photostability, non-biodegradable nature, and potential long-term cytotoxicity.[21,22] To date, abundant organic phototherapy agents have been explored to overcome the problems of inorganic materials such as RC-BSA[23] and NIR dyes (ICG, IR-820, and IR-825).[24] However, the low photothermal conversion efficiency and instability of these organic photothermal agents are not beneficial for clinical PTT. Hence, the rational design and synthesis of multi-functional photosensitizers with high NIR absorption ability, excellent photostability and biocompatibility as well as high PTC efficiency, is crucial for achieving effective PTT.

Diketopyrrolopyrrole (DPP), a red organic dye with a planar chemical structure, has attracted widespread attention owing to its excellent photostability, high fluorescence quantum yield, and intense absorption in the visible region.[25,26] In addition, chemical modifications on the DPP carbonyl groups is a potential method to enlarge the conjugated π-system and lower the band gap of DPP ramification.[27,28]

Herein, a NIR aza-BODIPY-fused DPP-derived photosensitizer with enlarged π-conjugation, pyrrolopyrrole aza-BODIPY (**PPAB**), was designed and synthesized. Biocompatible **PPAB** NPs were obtained *via* reprecipitation, which presented great photostability, high PTC efficiency and precise tumor targeting ability. The intense absorption peak at 730 nm as well as high PTC efficiency of 47% makes **PPAB** NPs an excellent candidate as a high-efficiency photothermal agent. The photothermal effect and NIR fluorescence emission of **PPAB** NPs can also be utilized for PAI and NIR-FI, respectively. Compared to other reported DPP-based

[a] *Key Laboratory of Flexible Electronics (KLOFE) and Institute of Advanced Materials (IAM), Nanjing Tech University (NanjingTech), Nanjing 211800, China. E-mail: iamxcdong@njtech.edu.cn, iamjjshao@njtech.edu.cn*
[b] *Department of Radiology, Binzhou Medical University Hospital, Yantai, Shangdong, 264100, China. E-mail: zisetasong@sina.com*

† Electronic supplementary information (ESI) available: Experimental details and supplementary figures. See DOI: 10.1039/c8cc07768a

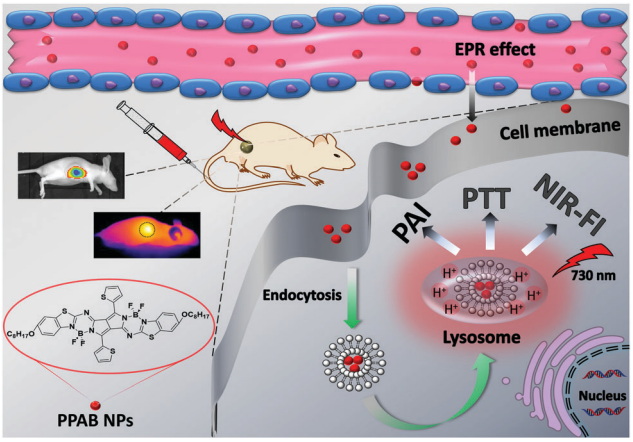

Scheme 1 Schematic illustration of **PPAB** NPs for NIR-FI/PAI imaging guided PTT.

organic NPs,[26,29–31] **PPAB** NPs possessed a higher PTC efficiency, thus making them a potential therapeutic agent for PAI and NIR-FI guided PTT (Scheme 1).

The synthetic route for **PPAB** is shown in Scheme S1 (ESI†). The heteroaromatic amine **2** was synthesized from 2-amino-6-hydroxybenzothiazole through an O-alkylation reaction. Compound **2** reacted with the DPP unit through a $TiCl_4$-mediated condensation and boron trifluoride diethyl ether complex addition, resulting in a quite straightforward synthesis of the aza-BODIPY fused DPP derivative. Subsequently, **PPAB** NPs were prepared through a reprecipitation approach. As shown in Fig. 1a, spherical **PPAB** NPs with an average particle size of 90 ± 7 nm were confirmed by dynamic light scattering and transmission electron microscopy. Therefore, **PPAB** NPs are a perfect therapeutic agent for *in vivo* passive tumor targeting based on the EPR effect.[32] The UV-vis absorption spectra (Fig. 1b) shows that **PPAB** and **PPAB** NPs displayed an intense NIR absorption with the max-absorption peak at 698 nanometer in DCM and 752 nanometer in an aqueous solution.

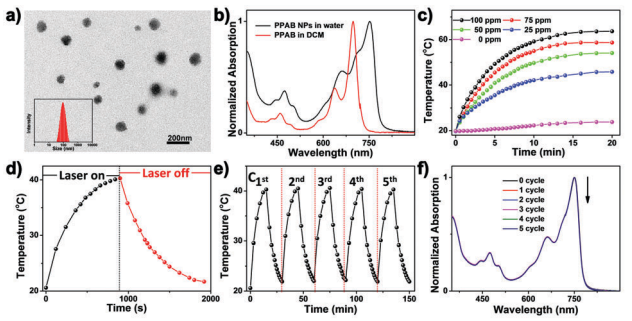

Fig. 1 (a) TEM image of **PPAB** NPs. Inset: Diameter distribution of **PPAB** NPs. (b) UV-vis absorption spectra of **PPAB** in DCM and **PPAB** NPs in water. (c) Temperature elevation curves of **PPAB** NPs at different concentrations (730 nm, 0.75 W cm^{-2}). (d) Photothermal response of **PPAB** NPs in an aqueous solution (25 ppm) under irradiation with a NIR laser (730 nm, 0.75 W cm^{-2}, 15 min) and after the laser was turned off. (e) Temperature profiles of **PPAB** NPS in an aqueous solution for five alternative ON/OFF cycles. (f) UV-vis absorption spectra of **PPAB** NPs after each ON/OFF cycle.

In addition, **PPAB** NPs displayed a wide absorption range of 500–800 nm in aqueous solution, which is preferred for high-efficiency PTT. **PPAB** NPs presented a fluorescence band from 670 to 780 nm with a maximum peak at 750 nm (Fig S1, ESI†) located in the NIR region, which enables **PPAB** NPs to be used for *in vivo* NIR fluorescence imaging.

Taking the excellent NIR absorption ability of PPAB NPs into consideration, we investigated their photothermal property. As shown in Fig. 1c, the temperature of the PPAB NPs aqueous solution increased with extended irradiation time and a higher concentration. The temperature of the PPAB NPs aqueous solution (100 ppm) apace rose from 19.8 °C to 49.3 °C in 5 min exposure under a 730 nm laser irradiation (0.75 W cm^{-2}). The temperature of pure water remained almost unchanged, confirming the excellent photothermal effect of **PPAB** NPs. Additionally, the temperature rate of the **PPAB** NPs aqueous solution could be accelerated by increasing the laser power density (Fig. S2, ESI†). The PTC efficiency of **PPAB** NPs was calculated to be 47% (Fig. 1d and Fig. S3, ESI†),[33] which is much higher than the PTC efficiencies of Au NRs (21%),[34] black phosphorus (28.4%),[35] and melanin nanosphere (40%).[36] These results further support the great potential of **PPAB** NPs as a high-efficiency photothermal agent.

It is well known that the photo-stability is a vital factor for phototherapy agents.[22] To investigate the photothermal stability of **PPAB** NPs, 1 mL samples were irradiated with a 730 nm laser (0.75 W cm^{-2}). After 15 min, the laser was turned off to cool the system. The UV-vis absorption spectra of **PPAB** NPs were recorded after each ON/OFF cycle. Surprisingly, as shown in Fig. 1e and f, after five ON/OFF cycles, **PPAB** NPs still maintained a high photothermal effect and the UV-vis absorbance showed no significant change, indicating their good photostability and photothermal stability. The particle size and absorbance of **PPAB** NPs did not show any significant change during the temperature increase (Fig. S4, ESI†). These results confirmed the excellent photothermal properties of **PPAB** NPs and highlighted their potential as a photothermal agent in clinic PTT.

The performance of **PPAB** NPs as a photothermal agent for *in vitro* ablation ability of cancer cells was assessed. HeLa cells were selected as tumor cell model. Live HeLa cell up-take experiments were conducted in the dark. Fig. 2a shows the fluorescence images of HeLa cells treated with **PPAB** NPs (60 ppm, 200 μL) after 12 hours incubation. The red fluorescence emission demonstrated that **PPAB** NPs were fully dispersed in the cell cytoplasm, suggesting an excellent bio-imaging property and effective up-take in HeLa cells. The typical MTT assay was used to verify and quantify the photothermal ablation ability of **PPAB** NPs. As shown in Fig. 2b, after incubation with PPAB NPs at various concentrations for one day in the dark, no proliferation inhibition and obvious cytotoxicity were observed, even when the NPs concentration was as high as 100 ppm. However, the cancer cells were efficiently killed by **PPAB** NPs under the exposure of a 730 nm laser illumination. More than 80% cells were killed when the concentration was as low as 30 ppm (Fig. 2c). These outcomes confirm that **PPAB** NPs have great potential as an efficient photothermal agent with low-toxicity for *in vivo* cancer treatment.

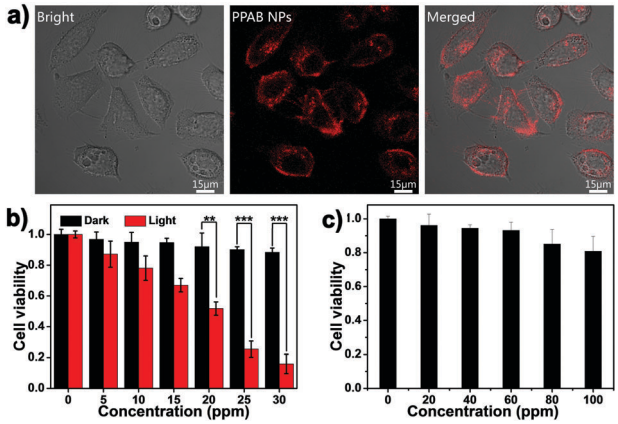

Fig. 2 (a) Confocal microscopy images of HeLa cells incubated with **PPAB** NPs (60 ppm) for 12 h. (b) Relative viabilities of HeLa cells after incubation with various concentrations of **PPAB** NPs (730 nm laser, 0.75 W cm^{-2}, 5 min, mean ± SD, $n = 5$, $^{**}P < 0.01$, $^{***}P < 0.001$). (c) Relative viabilities of HeLa cells after incubation with various concentrations of **PPAB** NPs for 24 h.

Encouraged by the above results, the *in vivo* imaging property of **PPAB** NPs was further investigated using the HeLa tumor-xenograft model. Photoacoustic imaging was utilized to monitor the dynamic accumulation of **PPAB** NPs in tumors. As shown in Fig. 3a, before the injection of **PPAB** NPs, no significant PA signal was observed from the tumor. However, the PA signal greatly increased 2 h later, indicating that the **PPAB** NPs accumulated in the tumor tissue. Over time, the **PPAB** NPs spread throughout the whole tumor tissue. The **PPAB** NPs reached the strongest PA intensity at the 10th hour (Fig. S5, ESI†) and maintained a high level of PA intensity after 24 hours. PA imaging indicated that **PPAB** NPs were capable of targeting tumors preferentially. As shown in Fig. 3b, the temperature of the tumor sites increased to 49.4 °C after an 8 min irradiation, which was high enough to kill the tumor cells *in vivo*. In the control group, the temperature of the tumor site slightly increased under the same laser condition when the mice were injected with PBS. As shown in Fig. 3c, after systemic administration of the **PPAB** NPs *via* tail vein injection, feeble fluorescence was detected within the first 2 h when irradiated with a 700 nm laser. The NIR fluorescence intensity increased over time and still maintained a high fluorescence signal after 24 hours, indicating that **PPAB** NPs not only efficiently accumulated at the tumor sites, but also had a long retention time *in vivo*. The maximum fluorescence signal occurred after the 6th hour (Fig. S6, ESI†), suggesting that 6 h to 12 h post-injection was the best time to treat the tumor-bearing mice. *In vitro* data further revealed that the tumor had the strongest NIR fluorescence after 24 h, followed by the liver. No significant NIR fluorescence could be detected in other primary organs. These *in vitro* and *in vivo* imaging data verified that **PPAB** NPs possessed excellent tumor accumulation ability and could be metabolized by liver. The PS NPs can accumulate efficiently in tumors. The mild hyperthermia induced by the conversion between light energy and heat energy during the PTT process improves the permeability of the vascular cell membrane and enhances vascular perfusion.[37] Overall, PAI as well as NIR-FI could offer powerful guidance for the phototherapy of PPAB NPs.

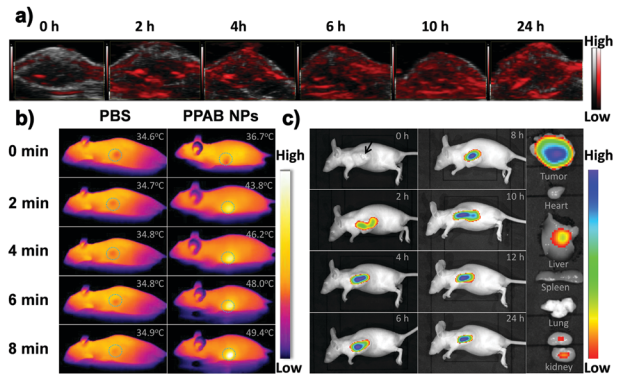

Fig. 3 (a) *In vivo* PA images in tumor sites after intravenous injection of **PPAB** NPs (50 ppm, 100 μL). (b) Photothermal images of tumor-bearing mice exposed to laser irradiation for 8 min after the injection of PBS or **PPAB** NPs. (c) Fluorescence images of living mice bearing xenograft HeLa tumors at 0, 2, 4, 6, 8, 10, 12 and 24 h post-injection of **PPAB** NPs.

All the above results proved that **PPAB** NPs are excellent photothermal material with good tumor accumulation ability, high PTC efficiency, excellent photothermal stability, and low dark cytotoxicity. Herein, we demonstrated the *in vivo* photothermal therapy ability of the **PPAB** NPs. Once the tumor size reached 100 mm^3, HeLa tumor-bearing mice ($n = 5$) were randomly divided into four groups (control, laser only, **PPAB** NPs only, and **PPAB** NPs with the laser). There were totally 8 treatment cycles. Each treatment cycle lasted for 2 days. In the treatment group, **PPAB** NPs (50 ppm, 100 μL) were injected into HeLa tumor-bearing mice *via* the tail vein every other day. The tumor sites were irradiated with laser (730 nm, 0.75 W cm^{-2}, 5 min) for 6 hours after NPs administration. Mice in the control groups were subjected to administration with PBS only and the comparison group with laser irradiation only or NPs only. The tumor size and body weights of the mice were recorded before starting the next cycle. As shown in Fig. 4a and b, after PPAB NPs injection and irradiation, tumors were effectively ablated. No skin damage was observed at the tumor site (Fig. 4c). However, for the other three groups, the tumor volumes rapidly expanded over time and showed a steady tumor growth ratio. This finding indicated that **PPAB** NPs with or without irradiation could not hinder the tumor growth. Moreover, no recurrence was observed in the **PPAB** NPs-induced PTT group, even for 14 more days of feeding. The body weight of the treatment and control groups steadily increased (Fig. 4d), demonstrating that the use of **PPAB** NPs as a photothermal agent had no evident toxicity and that **PPAB** NPs possessed excellent biocompatibility. To further investigate the potential toxicity of **PPAB** NPs, all mice were sacrificed at the end of the treatment. The heart, liver, spleen, lung, kidney, and tumors were harvested for histological examination *via* H&E staining. No discernible necrosis was found in the tumor sections for the other three groups (Fig. S7, ESI†), thus demonstrating the negligible dark toxicity and prominent biocompatibility of **PPAB** NPs. There was no evidently visible tissue damage throughout the organs (Fig. S8, ESI†). This finding further

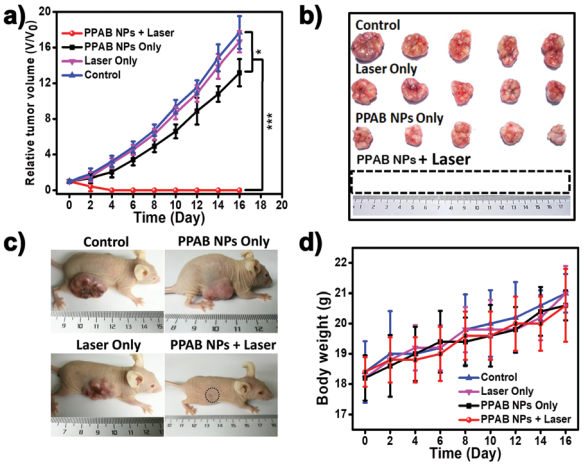

Fig. 4 (a) Tumor growth of various groups. Tumor volumes have been normalized to the initial sizes (mean ± SD, $n = 5$, $^{*}P < 0.05$, $^{***}P < 0.001$). (b) Photographs of excised tumors after various treatments. (c) Photographs of mice after 16 days treatment. (d) Body weight of various treatment groups.

confirmed the negligible-toxicity and remarkable biocompatibility of **PPAB** NPs *in vivo* as well as highlighted the great potential of **PPAB** NPs for PTT.

In summary, we have successfully synthesized an efficient photosensitizer, Pyrrolopyrrole aza-BODIPY (**PPAB**, for PAI- and NIR-FI-guided PTT). As-prepared **PPAB** NPs showed remarkable photostability in an aqueous solution and a high PTC efficiency of 47%. With the use of **PPAB** NPs as a photothermal agent, *in vitro* experiments demonstrated excellent tumor ablation ability, even at a low concentration. For *in vivo* PTT, **PPAB** NPs did not cause any significant toxicity in mice. Results demonstrated that 100% tumor elimination was realized under a 730 nm laser (0.75 W cm^{-2}). It is believed that **PPAB** NPs will play a prominent role in clinical dual-modality imaging-guided PTT in the near future.

The study was supported by the NNSF of China (61525402, 61775095, and 61604071), Jiangsu Provincial key research and development plan (BE2017741), and the Natural Science Foundation of Jiangsu Province (BK20161012).

Conflicts of interest

The authors of this manuscript have no conflicts of interest.

Notes and references

1 Q. Meng, J. Meng, W. Ran, J. Wang, Y. Zhai, P. Zhang and Y. Li, *ACS Nano*, 2018, **12**, 2789–2802.
2 W. Chen, J. Ouyang, H. Liu, M. Chen, K. Zeng, J. Sheng, Z. Liu, Y. Han, L. Wang, J. Li, L. Deng, Y. N. Liu and S. Guo, *Adv. Mater.*, 2017, **29**, 1603864.
3 Q. Lin, C. Bao, Y. Yang, Q. Liang, D. Zhang, S. Cheng and L. Zhu, *Adv. Mater.*, 2013, **25**, 1981–1986.
4 W. Fan, W. Bu, Z. Zhang, B. Shen, H. Zhang, Q. He, D. Ni, Z. Cui, K. Zhao, J. Bu, J. Du, J. Liu and J. Shi, *Angew. Chem.*, 2015, **54**, 14026–14030.
5 C. Dai, Y. Chen, X. Jing, L. Xiang, D. Yang, H. Lin, Z. Liu, X. Han and R. Wu, *ACS Nano*, 2017, **11**, 12696–12712.
6 D. Chen, Q. Tang, J. Zou, X. Yang, W. Huang, Q. Zhang, J. Shao and X. Dong, *Adv. Healthcare Mater.*, 2018, 1701272.
7 L. Cheng, W. He, H. Gong, C. Wang, Q. Chen, Z. Cheng and Z. Liu, *Adv. Funct. Mater.*, 2013, **23**, 5893–5902.
8 Y. Liu, K. Ai, J. Liu, M. Deng, Y. He and L. Lu, *Adv. Mater.*, 2013, **25**, 1353–1359.
9 P. Liang, Q. Tang, Y. Cai, G. Liu, W. Si, J. Shao, W. Huang, Q. Zhang and X. Dong, *Chem. Sci.*, 2017, **8**, 7457–7463.
10 X. Li, J. Kim, J. Yoon and X. Chen, *Adv. Mater.*, 2017, **29**, 1606857.
11 X. Cai, X. Jia, W. Gao, K. Zhang, M. Ma, S. Wang, Y. Zheng, J. Shi and H. Chen, *Adv. Funct. Mater.*, 2015, **25**, 2520–2529.
12 B. W. Michel, A. R. Lippert and C. J. Chang, *J. Am. Chem. Soc.*, 2012, **134**, 15668–15671.
13 Y. J. Liu, P. Bhattarai, Z. F. Dai and X. Y. Chen, *Chem. Soc. Rev.*, DOI: 10.1039/c8cs00618k.
14 J. Wang, J. Liu, Y. Liu, L. Wang, M. Cao, Y. Ji, X. Wu, Y. Xu, B. Bai, Q. Miao, C. Chen and Y. Zhao, *Adv. Mater.*, 2016, **28**, 8950–8958.
15 X. Zhu, H. K. Yip, X. Zhuo, R. Jiang, J. Chen, X. M. Zhu, Z. Yang and J. Wang, *J. Am. Chem. Soc.*, 2017, **139**, 13837–13846.
16 Z. Jiang, B. Dong, B. Chen, J. Wang, L. Xu, S. Zhang and H. Song, *Small*, 2013, **9**, 604–612.
17 L. Cheng, J. Liu, X. Gu, H. Gong, X. Shi, T. Liu, C. Wang, X. Wang, G. Liu, H. Xing, W. Bu, B. Sun and Z. Liu, *Adv. Mater.*, 2014, **26**, 1886–1893.
18 T. Liu, C. Wang, X. Gu, H. Gong, L. Cheng, X. Shi, L. Feng, B. Sun and Z. Liu, *Adv. Mater.*, 2014, **26**, 3433–3440.
19 S. S. Chou, B. Kaehr, J. Kim, B. M. Foley, M. De, P. E. Hopkins, J. Huang, C. J. Brinker and V. P. Dravid, *Angew. Chem.*, 2013, **52**, 4160–4164.
20 Y. W. Chen, Y. L. Su, S. H. Hu and S. Y. Chen, *Adv. Drug Delivery Rev.*, 2016, **105**, 190–204.
21 J. Qi, Y. Fang, R. T. K. Kwok, X. Zhang, X. Hu, J. W. Y. Lam, D. Ding and B. Z. Tang, *ACS Nano*, 2017, **11**, 7177–7188.
22 C. Kanimozhi, N. Yaacobi-Gross, K. W. Chou, A. Amassian, T. D. Anthopoulos and S. Patil, *J. Am. Chem. Soc.*, 2012, **134**, 16532–16535.
23 B. Zhou, Y. Li, G. Niu, M. Lan, Q. Jia and Q. Liang, *ACS Appl. Mater. Interfaces*, 2016, **8**, 29899–29905.
24 A. Tang, C. Zhan, J. Yao and E. Zhou, *Adv. Mater.*, 2017, **29**, 1600013.
25 J. Schmitt, V. Heitz, A. Sour, F. Bolze, H. Ftouni, J. F. Nicoud, L. Flamigni and B. Ventura, *Angew. Chem.*, 2015, **54**, 169–173.
26 Y. Cai, W. Si, W. Huang, P. Chen, J. Shao and X. Dong, *Small*, 2018, **14**, 1704247.
27 K. Miki, A. Enomoto, T. Inoue, T. Nabeshima, S. Saino, S. Shimizu, H. Matsuoka and K. Ohe, *Biomacromolecules*, 2017, **18**, 249–256.
28 S. Shimizu, T. Iino, A. Saeki, S. Seki and N. Kobayashi, *Chem. – Eur. J.*, 2015, **21**, 2893–2904.
29 Y. Cai, P. Liang, Q. Tang, W. Si, P. Chen, Q. Zhang and X. Dong, *ACS Appl. Mater. Interfaces*, 2017, **9**, 30398–30405.
30 Y. Cai, Q. Tang, X. Wu, W. Si, Q. Zhang, W. Huang and X. Dong, *ACS Appl. Mater. Interfaces*, 2016, **8**, 10737–10742.
31 Y. Cai, Q. Tang, X. Wu, W. Si, W. Huang, Q. Zhang and X. Dong, *ChemistrySelect*, 2016, **1**, 3071–3074.
32 J. Zhou, M. Li, Y. Hou, Z. Luo, Q. Chen, H. Cao, R. Huo, C. Xue, L. Sutrisno, L. Hao, Y. Cao, H. Ran, L. Lu, K. Li and K. Cai, *ACS Nano*, 2018, **12**, 2858–2872.
33 Y. Yuan, Z. Wang, P. Cai, J. Liu, L. D. Liao, M. Hong, X. Chen, N. Thakor and B. Liu, *Nanoscale*, 2015, **7**, 3067–3076.
34 D. K. Roper, W. Ahn and M. Hoepfner, *J. Phys. Chem. C*, 2007, **111**, 3636–3641.
35 Z. Sun, H. Xie, S. Tang, X. F. Yu, Z. Guo, J. Shao, H. Zhang, H. Huang, H. Wang and P. K. Chu, *Angew. Chem.*, 2015, **54**, 11526–11530.
36 Z. Zha, X. Yue, Q. Ren and Z. Dai, *Adv. Mater.*, 2013, **25**, 777–782.
37 G. Kong, R. D. Braun and M. W. Dewhirst, *Cancer Res.*, 2001, **61**, 3027.